Dust-acoustic wave modulation in the presence of superthermal ions

N. S. Saini[a] and I. Kourakis[b]
Centre for Plasma Physics, Department of Physics and Astronomy, Queen's University Belfast, BT7 1NN Northern Ireland, United Kingdom

(Received 22 August 2008; accepted 28 October 2008; published online 1 December 2008)

A study is presented of the nonlinear self-modulation of low-frequency electrostatic (dust acoustic) waves propagating in a dusty plasma, in the presence of a superthermal ion (and Maxwellian electron) background. A kappa-type superthermal distribution is assumed for the ion component, accounting for an arbitrary deviation from Maxwellian equilibrium, parametrized via a real parameter κ. The ordinary Maxwellian-background case is recovered for $\kappa \to \infty$. By employing a multiple scales technique, a nonlinear Schrödinger-type equation (NLSE) is derived for the electric potential wave amplitude. Both dispersion and nonlinearity coefficients of the NLSE are explicit functions of the carrier wavenumber and of relevant physical parameters (background species density and temperature, as well as nonthermality, via κ). The influence of plasma background superthermality on the growth rate of the modulational instability is discussed. The superthermal feature appears to control the occurrence of modulational instability, since the instability window is strongly modified. Localized wavepackets in the form of either bright-or dark-type envelope solitons, modeling envelope pulses or electric potential holes (voids), respectively, may occur. A parametric investigation indicates that the structural characteristics of these envelope excitations (width, amplitude) are affected by superthermality, as well as by relevant plasma parameters (dust concentration, ion temperature). © *2008 American Institute of Physics*. [DOI: 10.1063/1.3033748]

I. INTRODUCTION

Dust is a ubiquitous component of space and astrophysical environments occurring, for example, in planetary rings, comets, the Earth's ionosphere, interstellar molecular clouds, and circumstellar disks.[1–5] Dusty plasmas are ionized gases containing small (micron to submicron sized) charged particles of solid matter (dust grains).[4,5] The study of dusty plasmas also has a broad range of applications in industry and microelectronics.[6,7]

Because of the intriguing and often surprising results of the interaction between dust particles and plasmas, this has evolved into an important area of research. Dusty plasmas are known to support new electrostatic modes, which were predicted theoretically and also confirmed experimentally.[4,5,8–11] The dust ion-acoustic wave (DIAW) (Ref. 9) is the usual ion-acoustic mode modified by the presence of dust particles. The dust-acoustic wave (DAW),[8] of importance for us here, is sustained due to the restoring force provided by the plasma thermal pressure while inertia is due to the dust mass. The DAW/DIAW propagates as linear normal modes whose phase velocity is much larger than the dust thermal velocity.

A number of observations clearly indicate the presence of superthermal electron and ion populations in various laboratory[12] and space[13–18] plasmas environments. Superthermal particles may arise due to the effect of external forces acting on the natural space environment plasmas or to wave-particle interaction. The high-energy tail appearing in the corresponding distribution function(s) is conveniently modelled via a nonthermal distribution function. Based on theoretical studies in both space and laboratory plasmas, it has been observed that a plasma in the presence of superthermal particles suffers velocity-space diffusion.[19] This will lead to power law distribution at a velocity much higher than the electron thermal speed. For most space plasmas, the κ distribution[20] has been suggested to be appropriate for analysis, rather than a Maxwellian. The presence of a high-energy tail component in a kappa distribution considerably changes the rate of resonant energy transfer between particles and plasma waves, so that the conditions for the instability may be different for the two distributions.

Since the general form of the κ distribution and its relation to the Maxwellian distribution was first discussed by Vasyliunas,[20] it has been used to analyze and interpret spacecraft data on the Earth's magnetospheric plasma sheet,[21] the solar wind,[22] Jupiter,[23] and Saturn.[24] It has also been argued that many space plasmas can be modelled more effectively by the kappa distribution than by a superposition of Maxwellian distributions.[13–18,25–31] The κ distribution obeys an inverse power law at high velocities. For all velocities, in the limit when the spectral index κ approaches large values, the distribution function approaches the Maxwellian one. In this sense, the κ distribution is a generalization of the Maxwellian distribution. As suggested by theoretical studies,[14,15,18,32] we shall consider the value of κ to be higher than $3/2$ throughout this investigation. On the other hand, following Ref. 14 we shall assume κ to take any real value above $3/2$ (unlike in Ref. 13, where only integer κ was considered).

Despite the focus of extensive recent work on the effects of superthermal particles,[25–31] and in contrast with earlier models for nonthermal plasmas (e.g., based on the Cairns

[a]Electronic mail: nssaini@yahoo.com; ns.saini@qub.ac.uk.
[b]Electronic mail: i.kourakis@qub.ac.uk.

ansatz, see Refs. 33–35), the dynamics of nonlinear wavepackets propagating against a κ-distributed background have not yet been investigated, to the best of our knowledge. The aim of this paper is to fill in this gap. We shall study the dynamics of modulated dust-acoustic wavepackets in a dusty plasma composed of three distinct particle populations, namely inertial dust, Maxwellian electrons and ions obeying a kappa distribution function; the three species will be denoted by d, e, and i, respectively. In the present investigation, we have considered dust grains with constant charge since the typical time scales for the charging are much shorter than the dust-acoustic period as experimental and *ab initio* theoretical investigations suggest.[36] This is true in particular for quiescent (nonturbulent) situations with large dust grains and/or high plasma density (see the discussion in Ref. 36). Interestingly, a constant charge implies that collisionless damping[37] is not relevant in this parameter range. Therefore, we have chosen to model dust-acoustic waves via a dissipationless model. Dust charge dynamics may be added later (yet beyond our scope here).

Furthermore, we assume that electrons are lighter than ions, may relax faster to a Maxwellian equilibrium, while ions sustain their superthermal character longer. Thus, in qualitative agreement with, e.g., Ref. 35, we consider only ions to be superthermal. Admittedly, electrons may accelerate easily, and thus develop a tail in their distribution. This will be covered by an extension of the present work, which is underway.

The layout of this article goes as follows: In Sec. II, we present the model equations. Perturbation analysis is carried out in Sec. III and expressions for the dispersion relation and group velocity are derived. In Sec. IV, we derive a nonlinear Schrödinger equation. The fundamental information for a modulational stability analysis and for an investigation of the occurrence of localized envelope excitations is provided in Sec. V. A parametric investigation for either negatively or positively charged dust particles is presented in Secs. VI and VII, respectively. Section VIII is devoted to the conclusions of the results and discussion.

II. MODEL EQUATIONS

According to the model description above, we consider a simple dust-fluid model

$$\frac{\partial n_d}{\partial t} + \nabla \cdot (n_d \mathbf{u_d}) = 0, \tag{1}$$

$$\frac{\partial \mathbf{u_d}}{\partial t} + \mathbf{u_d} \cdot \nabla \mathbf{u_d} = -\frac{q_d}{m_d} \nabla \Phi, \tag{2}$$

$$\nabla^2 \Phi = -4\pi e(n_i Z_i - n_e + s n_d Z_d), \tag{3}$$

where n_d, $\mathbf{u_d}$, and Φ are the dust number density, the dust mean velocity, and the electric potential, respectively. m_α and q_α ($\alpha = e,i,d$) denote the mass and charge of electrons ($q_e = -e$), ions ($q_i = +Z_i e$) and heavy dust particulates ($q_d = sZ_d e$) with $s = \pm 1 = q_d/|q_d|$, respectively. Either a negative or a positive dust charge $q_d = sZ_d e$ can be accommodated in this description for $s = -1$ or $+1$, respectively. Overall charge neutrality at equilibrium is

$$n_{i0} Z_i - n_{e0} + s n_{d0} Z_{d0} = 0, \tag{4}$$

where $n_{\alpha 0}$ (for $\alpha = e,i,d$) are the unperturbed electron, ion, and dust number densities, respectively, and Z_{d0} is the unperturbed charge state of the dust grains.

We shall adopt a kappa-distribution for ions, by relying on the notation in Ref. 32 (wherein the fundamental algebra is expressed in detail). The number density for ions is accordingly expressed as

$$n_i = n_{i0}\left(1 + \frac{Z_i e \Phi}{\kappa k_B T_i}\right)^{-\kappa + 1/2}, \tag{5}$$

where κ is a real parameter measuring deviation from Maxwellian equilibrium (recovered for κ infinite). We use the expansion[32]

$$\left(1 + \frac{x}{\kappa}\right)^{-\kappa - 1} \approx e^{-x}\left[1 - \left(\frac{x}{\kappa}\right) + \frac{\kappa}{2}\left(\frac{x}{\kappa}\right)^2 - \frac{5\kappa}{6}\left(\frac{x}{\kappa}\right)^3 + \frac{\kappa^2}{8}\left(\frac{x}{\kappa}\right)^4 \cdots\right], \tag{6}$$

where $x = Z_i e \Phi / k_B T_i$. Combining Eqs. (5) and (6), the number density of ions takes the form as

$$n_i = n_{i0}(1 + b_1 \Phi + b_2 \Phi^2 + b_3 \Phi^3 + \cdots). \tag{7}$$

The coefficients b are given by

$$b_1 = \beta_1 \frac{Z_i e}{k_B T_i}, \quad b_2 = \beta_2 \left(\frac{Z_i e}{k_B T_i}\right)^2, \quad \text{and } b_3 = \beta_3 \left(\frac{Z_i e}{k_B T_i}\right)^3, \tag{8}$$

where

$$\beta_1 = \left(\frac{1}{2\kappa} - 1\right), \quad \beta_2 = \frac{1}{2} - \frac{9}{8\kappa^2},$$

$$\text{and} \quad \beta_3 = \left(-\frac{1}{6} - \frac{1}{4\kappa} + \frac{25}{24\kappa^2} - \frac{7}{16\kappa^3}\right), \tag{9}$$

i.e., in general,

$$b_m = \beta_m \left(\frac{Z_i e}{k_B T_i}\right)^m \quad \text{for } m = 1,2, \ldots . \tag{10}$$

Note that the Maxwellian limit is readily obtained upon setting $\kappa \to \infty$, which leads to

$$\beta_m = (-1)^m \frac{1}{m!} \quad \text{for } m = 1,2,3, \ldots . \tag{11}$$

The number density for electrons is given by

$$n_e = n_{e0}(1 + b_{em} \Phi^m), \tag{12}$$

where

$$b_{em} = \frac{1}{m!}\left(\frac{e}{k_B T_e}\right)^m \quad \text{for } m = 1,2,3, \ldots . \tag{13}$$

We shall consider wave propagation along $\hat{x}$, and will assume that all quantities vary along $\hat{x}$ only. After introduc-

ing the kappa distribution function, the normalized continuity, momentum, and Poisson's equations are written in a dimensionless form as

$$\frac{\partial n}{\partial t}+\frac{\partial (nu)}{\partial x}=0, \tag{14}$$

$$\frac{\partial u}{\partial t}+u\frac{\partial u}{\partial x}=-s\frac{\partial \phi}{\partial x}, \tag{15}$$

$$\frac{\partial^2 \phi}{\partial x^2}\approx -s(n-1)+c_1\phi+c_2\phi^2+c_3\phi^3, \tag{16}$$

where terms higher than ϕ^3 are omitted. The fluid velocity u_d, the particle density n_d, and the electric potential Φ are scaled as $u=u_d/v_d$, $n=n_d/n_{d0}$ (n_{d0} is the equilibrium dust density), and $\phi=|q_d|\Phi/(k_BT_{\rm eff})$. The characteristic dust speed scale is $v_d\equiv(k_BT_{\rm eff}/m_d)^{1/2}=\omega_{p,d}\lambda_{D,{\rm eff}}$. Space and time variables are scaled over the effective Debye length given as $\lambda_{D,{\rm eff}}=(k_BT_{\rm eff}/4\pi n_{d0}Z_d^2e^2)^{1/2}$ and the characteristic dust period (inverse dust plasma frequency) $\omega_{p,d}^{-1}=(4\pi n_{d0}q_d^2/m_d)^{-1/2}$.

The coefficients entering Poisson's equation (16) are

$$c_1=\frac{s}{(1-\mu)Z_d}\left(Z_i\beta_1\frac{T_{\rm eff}}{T_i}-\mu\frac{T_{\rm eff}}{T_e}\right),$$

$$c_2=\frac{s}{(1-\mu)Z_d^2}\left(Z_i^2\beta_2\frac{T_{\rm eff}^2}{T_i^2}-\frac{\mu}{2}\frac{T_{\rm eff}^2}{T_e^2}\right), \quad \text{and}$$

$$c_3=\frac{s}{(1-\mu)Z_d^3}\left(Z_i^3\beta_3\frac{T_{\rm eff}^3}{T_i^3}-\frac{\mu}{6}\frac{T_{\rm eff}^3}{T_e^3}\right). \tag{17}$$

In general, these dimensionless coefficients may be written as

$$c_m=\frac{s}{(1-\mu)Z_d^m}\left(Z_i^m\beta_{im}\frac{T_{\rm eff}^m}{T_i^m}-\frac{\mu}{m!}\frac{T_{\rm eff}^m}{T_e^m}\right) \quad \text{for } m=1,2,3, \tag{18}$$

or, expressed in reduced physical parameters, as

$$c_1=\frac{2\theta\kappa\mu-Z_i+2\kappa Z_i}{2\theta\kappa\mu+2\kappa Z_i},$$

$$c_2=s\frac{(\mu-1)[4\theta^2\kappa^2\mu+(9-4\kappa^2)Z_i^2]}{8\kappa^2(\theta\mu+Z_i)^2},$$

$$c_3=\frac{(\mu-1)^2[8\theta^3\kappa^3\mu+(2\kappa-3)(2\kappa-1)(7+2\kappa)Z_i^3]}{48\kappa^3(\theta\mu+Z_i)^3}. \tag{19}$$

The ion-to-electron temperature ratio is given as

$$\theta=\frac{T_i}{T_e}.$$

Finally, we have defined the dimensionless dust parameter as

$$\mu=\frac{n_{e0}}{Z_in_{i0}}=1+s\frac{Z_{d0}n_{d0}}{Z_in_{i0}}.$$

Notice that μ below (above) unity denotes negative (positive) dust. The effective temperature is given as

$$\frac{1}{T_{\rm eff}}=\frac{n_{i0}Z_i^2}{n_{d0}Z_d^2}\frac{1}{T_i}+\frac{n_{e0}}{n_{d0}Z_d^2}\frac{1}{T_e}\equiv\frac{s}{(\mu-1)Z_d}\left(\frac{Z_i}{T_i}+\frac{\mu}{T_e}\right). \tag{20}$$

We note that the perturbation technique we will employ, goes up to ϵ^3, so the cubic term in Eq. (16) is important. To trace the effect of the cubic term, see how b_3 from Eqs. (8)–(17) or Eq. (19) affects the nonlinearity coefficient Q in Eq. (40) below.

III. PERTURBATION ANALYSIS

The system's state is described by the variables $\{A\}$ $(=n,u,\phi)$ at a given position x and time t. Let us consider a small deviation from the equilibrium state $A^{(0)}$ which is given by $n^{(0)}=1$ and $u^{(0)}=\phi^{(0)}=0$. Then we can write a general expression for the variables as

$$A=A^{(0)}+\sum_{m=1}^{\infty}\epsilon^mA^{(m)}, \tag{21}$$

where $\epsilon\ll 1$ is a small parameter. Here we will consider a general stretched (slow) space and time variables scaling as

$$X_m=\epsilon^m x, \quad \text{and } T_m=\epsilon^m t. \tag{22}$$

We have assumed that

$$A^{(m)}=\sum_{l=-m}^{m}A_l^{(m)}(X_m,T_m)\exp[il(kx-\omega t)]. \tag{23}$$

$A_l^{(m)}$ satisfies the reality condition $A_l^{(m)}=A_{-l}^{(m)*}$, where the asterisk denotes the complex conjugate. Substituting Eq. (23) into Eqs. (14)–(16) and using Eq. (22), we can find different expressions by isolating various orders in ϵ. The first order equations are

$$-i\omega n_1^{(1)}+iku_1^{(1)}=0, \tag{24}$$

$$-i\omega u_1^{(1)}+sik\phi_1^{(1)}=0, \tag{25}$$

$$sn_1^{(1)}-(k^2+c_1)\phi_1^{(1)}=0. \tag{26}$$

The solution for the first harmonics read as

$$n_1^{(1)}=s(k^2+c_1)\phi_1^{(1)}, \tag{27}$$

$$u_1^{(1)}=\frac{\omega}{sk}(k^2+c_1)\phi_1^{(1)}=\frac{\omega}{k}n_1^{(1)}. \tag{28}$$

We thus obtain the dispersion relation for dust-acoustic waves,

$$\omega^2=\frac{k^2}{k^2+c_1}. \tag{29}$$

One immediately notices the effect of the nonthermality (via κ), of the dust concentration (via μ) and of the plasma species temperature on the phase speed (for low k),

$$v_{\rm ph} = \frac{\omega}{k} \approx \left[\frac{2\kappa(\theta\mu + Z_i)}{2\kappa(\theta\mu + Z_i) - Z_i} \right]^{1/2}. \tag{30}$$

We note that c_1 can be shown to be positive (for all parameter values of physical interest), thus linear stability is ensured in Eq. (29).

At second order in ϵ, we expect to find expressions for the group velocity v_g, and for the zeroth and second harmonics. For $m=2$ and $l=1$, we need to impose a compatibility condition in the form

$$\frac{\partial \phi_1^{(1)}}{\partial T_1} + v_g \frac{\partial \phi_1^{(1)}}{\partial X_1} = 0, \tag{31}$$

where we have defined the group velocity $v_g(k) = \partial\omega/\partial k = \omega'(k)$, given by

$$v_g = c_1 \frac{\omega^3}{k^3}. \tag{32}$$

The expressions for the amplitudes corresponding to the first harmonics in order ϵ^2 are given by

$$n_1^{(2)} = s(k^2 + c_1)\phi_1^{(2)} - 2isk\frac{\partial \phi_1^{(1)}}{\partial X_1},$$

$$u_1^{(2)} = \frac{sk}{\omega}\phi_1^{(2)} - is\omega\frac{\partial \phi_1^{(1)}}{\partial X_1},$$

$$\phi_1^{(2)} = i\tilde{A}\frac{\partial \phi_1^{(1)}}{\partial X_1}, \tag{33}$$

where the choice of $\tilde{A}$ is arbitrary and we shall take it to be equal to zero. For $m=2$ and $l=2$, the evolution equations provide the amplitudes of the second order harmonics which are found to be proportional to $(\phi_1^{(1)})^2$. The expressions for these amplitudes are

$$n_2^{(2)} = C_1^{(22)}(\phi_1^{(1)})^2, \quad u_2^{(2)} = C_2^{(22)}(\phi_1^{(1)})^2, \quad \text{and}$$

$$\phi_2^{(2)} = C_3^{(22)}(\phi_1^{(1)})^2, \tag{34}$$

where

$$C_1^{(22)} = sc_2 + s(4k^2 + c_1)C_3^{(22)},$$

$$C_2^{(22)} = \frac{\omega}{k}[C_1^{(22)} - (k^2 + c_1)^2], \quad \text{and}$$

$$C_3^{(22)} = -\frac{c_2}{3k^2} + \frac{s(k^2 + c_1)^2}{2k^2}. \tag{35}$$

Now we also obtain (combining expressions for $m=2$, $l=0$ and $m=3$, $l=0$),

$$n_0^{(2)} = C_1^{(20)}|\phi_1^{(1)}|^2, \quad u_0^{(2)} = C_2^{(20)}|\phi_1^{(1)}|^2, \quad \text{and}$$

$$\phi_0^{(2)} = C_3^{(20)}|\phi_1^{(1)}|^2, \tag{36}$$

where

$$C_1^{(20)} = s[c_1 C_3^{(20)} + 2c_2],$$

$$C_2^{(20)} = -\frac{2\omega}{k}(k^2 + c_1) + v_g C_1^{(20)}, \quad \text{and}$$

$$C_3^{(20)} = \frac{2c_2 v_g^2 - s(k^2 + 3c_1)}{1 - c_1 v_g^2}. \tag{37}$$

Note that all physical parameters lead to an explicit dependence of all coefficients on μ, θ, and κ. The expected Maxwellian limit is recovered for $\kappa \to \infty$.[38,39]

IV. A NONLINEAR SCHRÖDINGER EQUATION FOR THE SLOWLY VARYING POTENTIAL AMPLITUDE

To third order in ϵ, the reduced equations for $l=1$ yield an explicit compatibility condition. This leads to an equation in the form

$$i\left[\frac{\partial \phi_1^{(1)}}{\partial T_2} + v_g \frac{\partial \phi_1^{(1)}}{\partial X_2} \right] + P\frac{\partial^2 \phi_1^{(1)}}{\partial X_1^2} + Q|\phi_1^{(1)}|^2 \phi_1^{(1)} = 0. \tag{38}$$

The dispersion coefficient P is given by

$$P = -\frac{3}{2}c_1\frac{\omega^5}{k^4}. \tag{39}$$

Note that the P is equal to $\partial^2\omega/2\partial k^2$, as expected. We note that P is always negative (since $c_1 > 0$ for all parameter values of interest), as reflected upon simple inspection of the dispersion curve(s) in Fig. 4 below.

The nonlinearity coefficient Q is given by

$$Q = \frac{\omega^3}{k^2}\left\{ c_2[C_3^{(20)} + C_3^{(22)}] + \frac{3}{2}c_3 \right\} - \frac{\omega}{2}[C_1^{(20)} + C_1^{(22)}] - k[C_2^{(22)} + C_2^{(20)}]. \tag{40}$$

It may be appropriate to consider the large wavelength behavior in the above coefficients, by considering the limit $k \ll 1$. A tedious yet straightforward algebraic study reveals that P vanishes for low k (as expected for an acoustic mode, where $\omega \sim k$ and $\omega'' \simeq 0$) as $P \simeq -p_0 k$, whereas Q diverges as $Q \simeq q_0/k$. This is in qualitative agreement with earlier theoretical considerations.[34,40] The real quantities p_0 and q_0, in fact both positive, are given by

$$p_0 = \frac{3}{2c_1^{3/2}} \tag{41}$$

and

$$q_0 = \frac{1}{12}\left(\frac{1}{c_1}\right)^{3/2}(2c_2 - 3sc_1^2)^2. \tag{42}$$

The total (first order) solution obtained for the electric potential is

$$\phi \simeq \phi_1^{(1)} = \psi(x,t)e^{i(kx-\omega t)} + \psi^*(x,t)e^{-i(kx-\omega t)}, \tag{43}$$

where the variation of $\psi(x,t)$ is assumed to be slower than that of $\exp[i(kx-\omega t)]$ [$\epsilon=1$ was formally set here, with the understanding that $\psi = \phi_1^{(1)} \ll 1$ remains small]. The compat-

ibility condition is now written in the form of a nonlinear Schrödinger (NLS) equation

$$i\left(\frac{\partial\psi}{\partial t}+v_g\frac{\partial\psi}{\partial x}\right)+P\frac{\partial^2\psi}{\partial x^2}+Q|\psi|^2\psi=0, \tag{44}$$

for the small, slowly varying amplitude $\psi(x,t)$. Performing a Galilean transformation, finally, the NLSE can be written in its standard form as

$$i\frac{\partial\psi}{\partial t}+P\frac{\partial^2\psi}{\partial x^2}+Q|\psi|^2\psi=0. \tag{45}$$

V. MODULATIONAL INSTABILITY AND ENVELOPE EXCITATIONS

The evolution of a wave whose amplitude obeys the nonlinear Schrödinger equation (45) essentially depends on the dispersion and nonlinearity coefficients, P and Q, respectively, whose analytical behavior can be investigated in terms of all relevant physical parameters.[40] Omitting details already exposed in the literature (see, e.g., in Ref. 40), we shall summarize the basis of the analysis to follow below, and will then proceed by an analytical investigation in terms of relevant parameters.

A. Modulational instability (MI)

The modulational instability of the envelope can be studied by considering a small perturbation of the wave's amplitude and studying the associated dispersion relation.[40] Assuming a small and slowly varying perturbation of the amplitude, which bears a magnitude A_0, a small frequency $\tilde{\omega}\ll\omega$, and a small wavenumber $\tilde{k}\ll k$, leads to a dispersion relation of the form

$$\tilde{\omega}^2=P^2\tilde{k}^2\left(\tilde{k}^2-2\frac{Q}{P}|A_0|^2\right). \tag{46}$$

It is straightforward to see that a negative sign for Q/P is required for wave amplitude (modulational) stability. On the other hand, a positive sign of Q/P allows for a random perturbation of the amplitude to grow, and may thus lead to wave collapse of blowup. Interestingly, wavepacket stability is always ensured in the large wavelength region (for $k\ll 1$); see expressions (41) and (42) in the previous section. The maximum growth rate of the instability equals $Q_\infty|A_0|^2$ and is attained for $\tilde{k}=|A_0|\sqrt{Q/P}=\tilde{k}_0$, while the instability window extends from $\tilde{k}$ equals to zero to $\sqrt{2}|A_0|\sqrt{Q/P}$. Details can be found in Refs. 40 and 41. It would be instructive to investigate the dependence of the MI growth rate on κ. From Eq. (46), we obtain the following expression for the growth rate (for a given value of κ, denoted by the subscript) as

$$\Gamma_\kappa=\alpha X\left(2\frac{\beta}{\alpha}-X^2\right)^{1/2}, \tag{47}$$

where $\Gamma_\kappa=\mathrm{Im}\,\tilde{\omega}/(Q_\infty|A_0|^2)$, $\alpha=P/P_\infty$, $\beta=Q/Q_\infty$, and $X=\tilde{k}\sqrt{P_\infty}/(|A_0|\sqrt{Q_\infty})$ with $P_\infty=P(\kappa\to\infty)$ and $Q_\infty=Q(\kappa\to\infty)$. Equation (47) should be compared to the following expression:

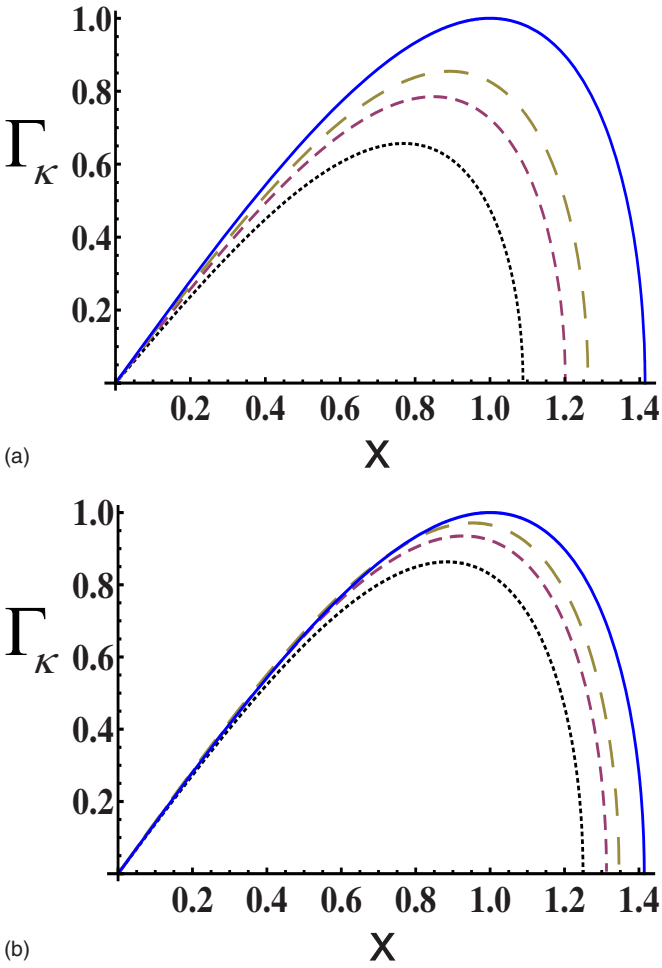

FIG. 1. (Color online) Variation of the growth rate Γ_κ (negative dust) with X for different values of κ with $s=-1$, $k=0.84$, and $\theta=0.1$. The dotted curve corresponds to $\kappa=2.0$, dashed curve to $\kappa=2.5$, long dashed curve to $\kappa=3.0$, and solid curve to $\kappa=\infty$. (a) $\mu=0.55$, and (b) $\mu=0.9$.

$$\Gamma_\infty=X(2-X^2)^{1/2}, \tag{48}$$

in the Maxwellian case ($\kappa\to\infty$), which presents a maximum at $(X_0,\Gamma_{\infty,\max})=(1,1)$, and a root at $(\sqrt{2},0)$. One is therefore interested in tracing the effect of κ on the maximum and on the MI window (interval of unstable values). The growth rate of the modulational instability (for negative dust) for different values of κ is depicted in Fig. 1. It is observed that the growth rate is significantly affected by the variation in the values of κ since its maximum value moves to $\Gamma_{\max}=\beta$ (viz. $\mathrm{Im}\,\tilde{\omega}=Q_\kappa|A_0|^2$) attained at $X_0=(\beta/\alpha)^{1/2}$ as the background becomes significantly superthermal (i.e., κ attaining low values). The instability window becomes the interval $[0,\sqrt{\alpha/(2\beta)}]$. A similar qualitative effect is witnessed in the presence of positive dust (see Fig. 2). We note that the effect on the growth rate may as well be the inverse one, depending on the relative magnitude of P and Q; see, e.g., in Fig. 2(b), where superthermality appears to increase the MI growth rate [upper curve in Fig. 2(b)]. One draws the conclusion that superthermality may control (and in fact prevent) the occurrence of modulational instability.

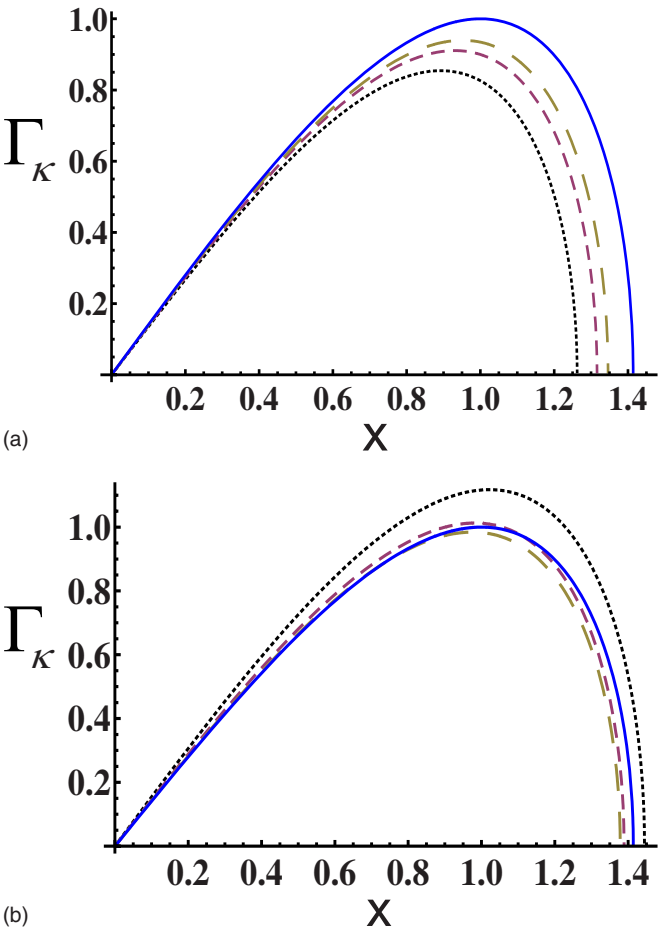

FIG. 2. (Color online) Variation of the growth rate Γ_κ (positive dust) with X for different values of κ with $s=+1$, $k=0.95$, and $\theta=0.1$. The dotted curve corresponds to $\kappa=1.6$, dashed curve to $\kappa=2.5$, long dashed curve to $\kappa=3.5$, and solid curve to $\kappa=\infty$. (a) $\mu=1.1$, and (b) $\mu=1.5$.

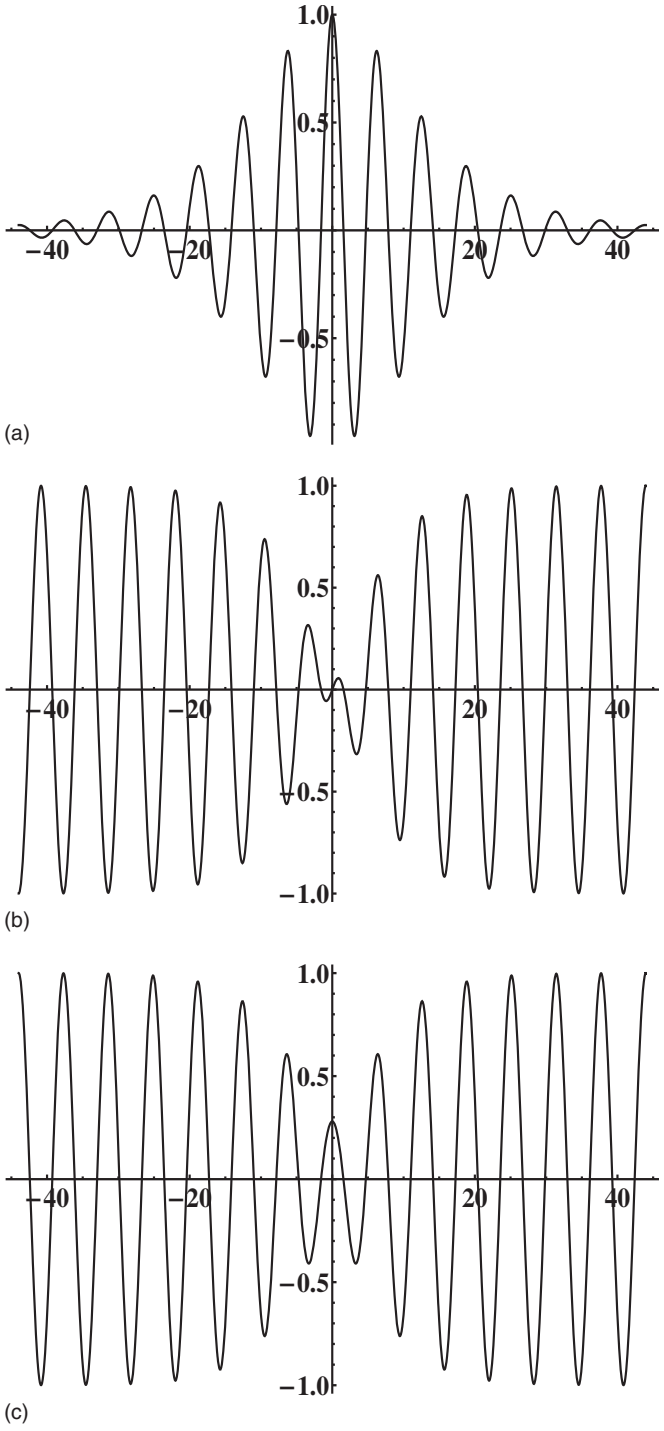

FIG. 3. Heuristic picture of envelope soliton solutions of the NLS Eq. (45) (arbitrary parameter values): (a) bright, (b) black, and (c) grey type envelope solitons are depicted.

B. Envelope solitons

A nonlinear analysis of the envelope dynamics, as modelled by the NLSE [Eq. (45)], reveals the existence of localized solutions in the form of envelope solitons of either the bright or dark type.[41–43] Omitting details,[41–43] we suggest that an appropriate quantity to investigate is the ratio Q/P, since its sign determines the type of envelope excitations (in addition to the MI of wavepackets; see above), while its (absolute) value $|Q/P|$ determines the envelope soliton characteristics. We summarize these key points below.

Bright versus dark solitons. Bright-type envelope solitons (pulses) occur when $Q/P>0$, and are essentially pulse-shaped envelopes confining the fast carrier wave; see Fig. 3(a). On the other hand, the case $Q/P<0$ is associated with *dark-type* excitations, manifested as localized envelope holes or voids in the center, amidst regions of constant amplitude in either sides (extended to both infinities); these excitations may either reach a vanishing amplitude in the center or a finite one (*black* or *grey* envelope solitons, respectively); see Figs. 3(b) and 3(c).

Soliton geometry. A detailed analysis in respect of electrostatic plasma modes can be found in Ref. 40, while analytical details and the derivation of these soliton solutions are extensively discussed in Refs. 42 and 43, so these are omitted here for brevity. It turns out that the soliton amplitude Ψ_0 and the soliton width L satisfy[40,42,43]

$$\Psi_0 L \sim (|Q/P|)^{1/2} \tag{49}$$

in both bright and dark cases. Note the qualitative distinction from $\psi_0 L^2=$constant which would be the KdV soliton case. This also suggests that for a given value of, say, potential amplitude Ψ_0, the envelope pulses will be wider in regions where the value of Q/P is higher, and vice versa.

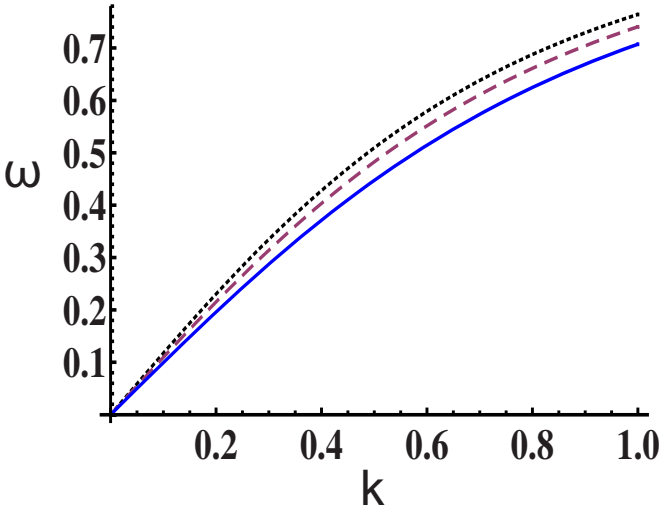

FIG. 4. (Color online) Variation of the carrier frequency ω with the wavenumber k for different values of the parameter κ, with $\mu=0.9$, θ $(=T_i/T_e)=0.1$, and $s=-1$ (negative dust). The dotted (upper) curve corresponds to $\kappa=1.6$, dashed (middle) curve to $\kappa=2.5$, and solid (lower) curve to $\kappa=\infty$.

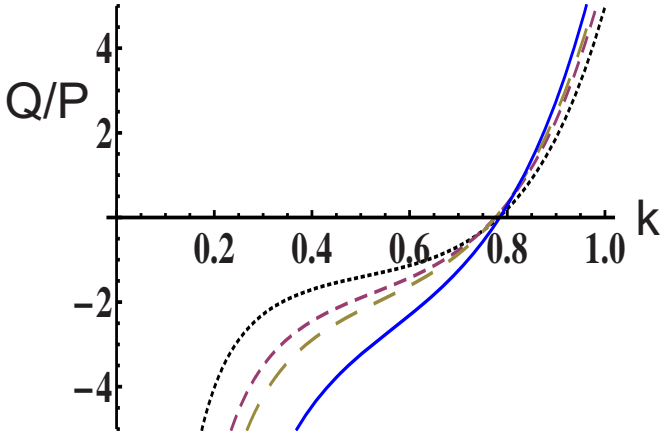

FIG. 5. (Color online) Variation of the NLSE coefficients ratio Q/P with the carrier wavenumber k for different values of κ and with $\mu=0.9$, $\theta=0.1$, and $s=-1$. The dotted curve corresponds to $\kappa=1.6$, dashed curve to $\kappa=2.5$, long dashed curve to $\kappa=3.5$, and solid curve to $\kappa=\infty$.

Summarizing, we may investigate the envelope soliton characteristics by plotting the ratio Q/P versus relevant parameters (see Figs. 5, 7, 9, and 11–13 below).

VI. PARAMETRIC INVESTIGATION: NEGATIVE DUST CHARGE

We have derived a nonlinear Schrödinger equation using a multiple scales (reductive perturbation) method for unmagnetized dusty plasma containing negative dust grains, Maxwellian electrons, and kappa distributed ions. Physically, both phase and group velocities of the wave are modified by the plasma parameters. This essentially entails a modification in the dispersive and nonlinear behavior of the plasma as a whole, which is manifested in the wavepacket's modulational profile. The effect of different physical parameters on the envelope dynamics, as manifested via the ratio Q/P (see discussion above), will be investigated below, in terms of relevant parameters, namely (i) the wavenumber k, (ii) the temperature ratio θ $(=T_i/T_e)$, (iii) the dust density parameter μ (recall that values below/above 1 stand for negative/positive dust), and finally (iv) the value of κ reflecting the deviation from Maxwellian distribution for the ions.

Effect of superthermality. We have analyzed the variation of ω with the wave number k [as given by the dispersion relation (29)] for different values of κ and keeping other parameters fixed ($\theta=0.1$ and $\mu=0.9$ in Fig. 4). It is seen that ω decreases as the value of κ increases. The solid curve corresponds to $\kappa\to\infty$ and shows that the value of ω is small as compare to other values of κ. Thus, deviation from a thermal (Maxwellian) distribution appears to enhance electrostatic oscillations.

We have investigated the stability profile by depicting the ratio Q/P versus k for different parameter values. We have determined in various regimes the critical wavenumber threshold k_{cr} (at which $Q/P=0$), which indicates where the instability sets in.

The variation of the ratio Q/P with k for different values of κ is shown in Fig. 5. The threshold k_{cr} bears a value around 0.77, which separates stable ($k<k_{cr}$, where $Q/P<0$) from unstable ($k>k_{cr}$, or $Q/P>0$) regions. Dark solitons occur in the former case, i.e., for large wavelengths, while bright envelope solitons occur in the latter region, i.e., for wavelengths shorter than $2\pi/k_{cr}$. In all cases, the infinite wavelength limit seems to predict stability, as physically expected.

In the stable region ($k<k_{cr}$) (see Fig. 5) the absolute value of the ratio Q/P decreases as κ decreases, for given k, and also decreases with k for given κ. Superthermality leads to narrower (in spatial extension) bright or dark envelope solitons, although the effect on the bright case is less important. The solid curve corresponds to $\kappa\to\infty$. Therefore, the higher the deviation from a thermal ion distribution, the narrower the electric potential envelope excitations will be. Note that this is also true in the unstable region ($k>k_{cr}$) and may thus be kept as a general result in both bright and dark envelope cases. However, higher values of k will bear narrower dark solitons or wider bright ones, in the respective regions (left and right in Fig. 5).

The dependence of the critical wavenumber k_{cr} on κ for different values of μ is depicted in Fig. 6. We see that k_{cr} decreases with κ (note the curves 4, 5, and 6 in Fig. 6, where $\mu<1$, i.e. for negative dust) and in fact reaches an asymptotic value for κ higher than, say, 5 or 6. This seems to be in agreement with earlier results,[12,14–18] which asserted that values of κ higher than 5 practically recover the Maxwellian limit. On the other hand, k_{cr} decreases if the value of μ goes lower (cf. curves 4–6 in Fig. 6), implying that addition of negative dust (i.e., a stronger deviation from unity from below) leads to a lower threshold, i.e., that instability sets in for lower wavenumbers.

Ion temperature effect. We have analyzed the effect of ion temperature on the modulational instability. Figure 7 depicts the dependence of the ratio Q/P on k for different values of the temperature ratio θ $(=T_i/T_e)$. An increase in the ion temperature seems to move the curve downwards (to

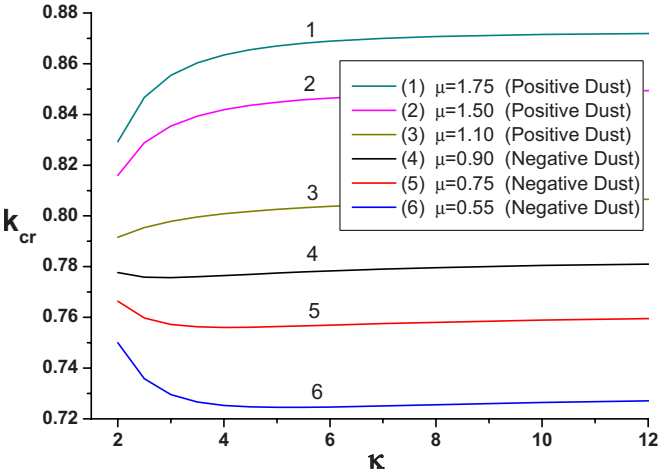

FIG. 6. (Color online) Variation of the instability (carrier wavenumber) threshold k_{cr} with κ for different values of (the dust parameter) μ and (temperature ratio) $\theta=0.1$.

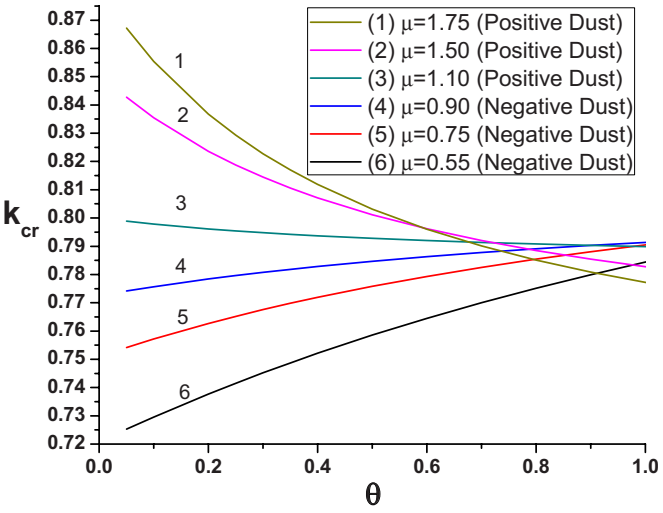

FIG. 8. (Color online) Variation of the instability (carrier wavenumber) threshold k_{cr} with θ for different values of μ and $\kappa=3$.

higher $|Q/P|$) in the stable region ($k<k_{cr}$, where $Q/P<0$), although it bears hardly any effect in the unstable one ($k>k_{cr}$, or $Q/P>0$). The threshold k_{cr} itself also increases with θ, as shown in Fig. 8; different curves correspond to different values of μ therein (only curves 4–6 in Fig. 8 are relevant to negative dust). Therefore, k_{cr} will be lower (and thus wavepackets will be stable in a narrower region) either for cooler ions or for stronger negative dust presence. Negative dust favors modulational instability, therefore (also see next paragraph).

Influence of the dust concentration. We have analyzed the stable and unstable regions with varying dust concentration. The variation of the ratio Q/P with k for different dust concentration parameter μ is shown in Fig. 9. It is noticed that an increase in negative dust concentration, i.e., as μ decreases, leads to smaller $|Q/P|$ in the stable region (i.e., smaller dark envelope solitons) but to a higher Q/P in the unstable one (thus wider bright envelopes). Furthermore, the k_{cr} value decreases with more negative dust (for lower μ), as also manifested in Fig. 10. The influence of the dust concentration on the stability profile seems to be more significant than that of other physical factors. This seems to be in qualitative agreement with previous results on nonthermal dusty plasmas, obtained via another model.[34]

VII. PARAMETRIC INVESTIGATION: POSITIVE DUST CHARGE

A presence of positive dust may be observed, e.g., in different regions in space, as in cometary tails,[3] in the upper mesosphere,[44] in Jupiter's magnetosphere,[3,45] etc., as in the laboratory.[46] This may be due to different charging mechanisms, such as, a flux of ultraviolet photons, thermionic emission or to a secondary emission of electrons from the dust grain surface, creating a deficit in electrons.[5] Dusty plasmas with positively charged dust grains have been studied theoretically[47] and also experimentally.[46] Interestingly, the presence of positive dust grains in a dusty plasma was recently shown to modify the basic properties of solitary potential structures and lead to a possible coexistence of posi-

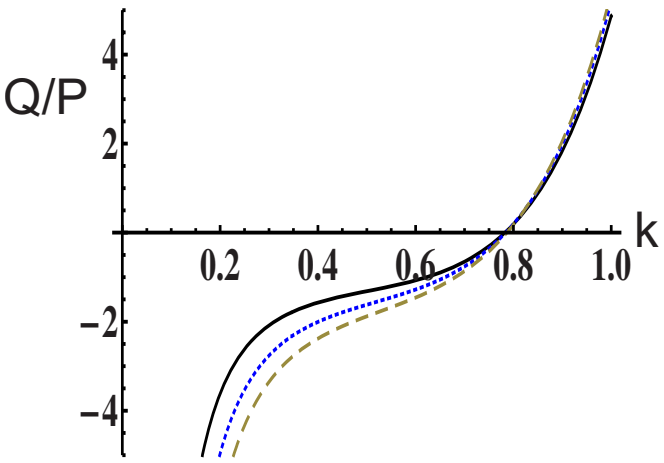

FIG. 7. (Color online) Variation of the ratio Q/P with the carried wavenumber k for different values of θ, with $\kappa=1.6$, $\mu=0.9$, and $s=-1$. Solid curve corresponds to $\theta=0.02$, dotted curve to $\theta=0.2$, and dashed curve to $\theta=0.5$.

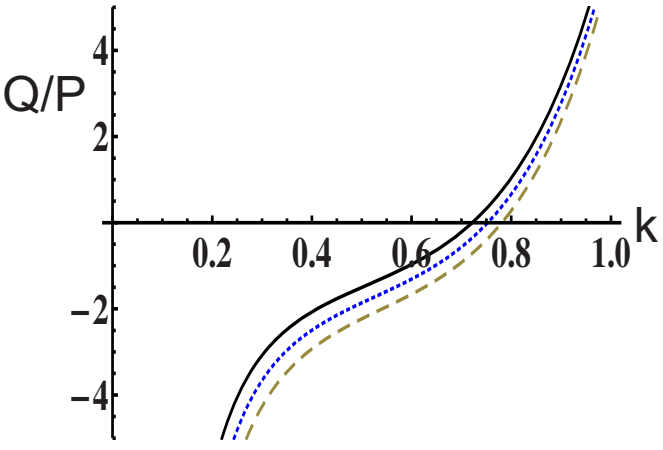

FIG. 9. (Color online) Variation of the ratio Q/P with the carrier wavenumber k for different values of μ and with $\kappa=3.5$, $\theta=0.1$, and $s=-1$. The solid curve corresponds to $\mu=0.55$, dotted curve to $\mu=0.75$, and dashed curve to $\mu=0.95$.

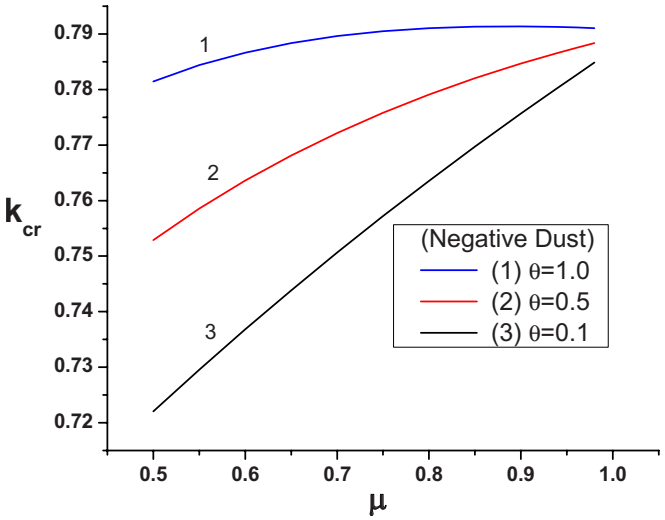

FIG. 10. (Color online) Variation of the instability (carrier wavenumber) threshold k_{cr} with the dust parameter μ (negative dust) for different values of θ and $\kappa=3$.

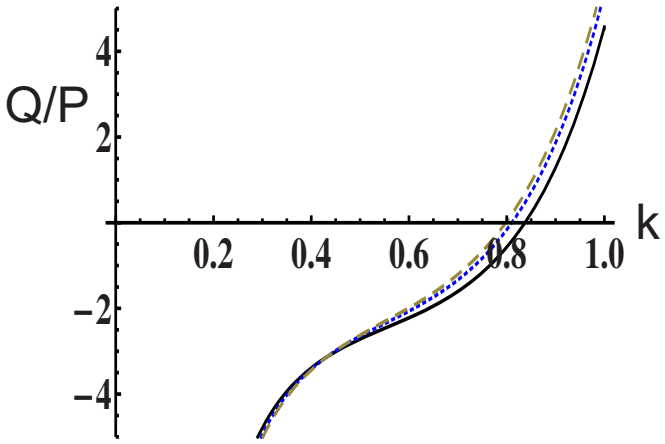

FIG. 12. (Color online) Variation of the ratio Q/P with the carrier wavenumber k for different values of θ and with $\kappa=2.5$, $\mu=1.5$, and $s=+1$ (positive dust). The solid curve corresponds to $\theta=0.05$, dotted curve to $\theta=0.3$, and dashed curve to $\theta=0.5$.

tive and negative solitary potential structures.[48,49] Given this feedback, we have extended our analysis to an investigation of the modulational profiles of electrostatic wavepackets in the presence of a positive dust component.

Effect of superthermality. As previously said (and depicted in Fig. 4), the frequency ω decreases with lower values of κ (i.e., larger deviation from a thermal ion distribution); this is also valid in the presence of positive dust, for any value of $\mu>1$ (corresponding plot omitted for brevity).

In Fig. 11, it is seen that the critical value k_{cr} now lies near ≈ 0.80 for finite value of κ (i.e., is generally higher than for negative dust), though it decreases with lower κ: note the upper curves 1–3 in Fig. 6 (for $\mu>1$). In the stable region ($Q/P<0$), where dark solitons exist, $|Q/P|$ decreases with lower κ, for given k, and also vice versa. Superthermality leads to narrower (in spatial extension) bright or dark envelope solitons, but practically no change for bright solitons. In Fig. 11, the solid curve corresponds to $\kappa\to\infty$ (Maxwellian limit). Still, the effect on k_{cr} is easier to observe than for a negative dust charge. Again, superthermality seems to affect the characteristics of dark solitons, which become narrower for superthermal ions, although the inverse effect born on the bright solitons (in the unstable region) is not that dramatic; however, Q/P definitely increases with k, suggesting that bright solitons of a given width will be larger at higher k (i.e., for smaller wavelength). As seen in Fig. 6 (upper 3 curves for positive dust), k_{cr} now increases with higher κ (contrary to the negative dust case), up to certain asymptotic values beyond which the Maxwellian limit is recovered.

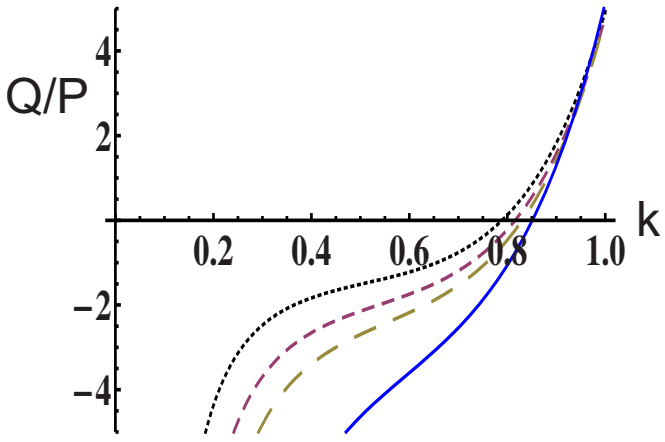

FIG. 11. (Color online) Variation of the ratio Q/P with the carrier wavenumber k for different values of κ and with $\mu=1.5$, $\theta=0.1$, and $s=+1$ (positive dust). The dotted curve corresponds to $\kappa=1.6$, dashed curve to $\kappa=2$, long dashed curve to $\kappa=2.5$, and solid curve to $\kappa=\infty$.

Ion temperature effect. The effect of the ion temperature on the modulational instability profile is analyzed in Fig. 12, which depicts the dependence of the ratio Q/P on k for different values of θ ($=T_i/T_e$). As the ion temperature increases, the (absolute) value of Q/P goes lower/higher in the negative/positive region (i.e., left/right, respectively), suggesting that dark/bright envelope solitons will be smaller/larger (respectively). The instability threshold is clearly seen to decrease for higher T_i, as confirmed in Fig. 8 (see upper 3 curves therein). This is contrary to the negative dust case; for positive dust, ion heating enhances instability at lower k.

Influence of the positive dust concentration. Figure 13 shows the variation of the ratio Q/P with k for different values of μ (hence the dust concentration). There is a rather significant modification in k_{cr} by changing μ. In fact, k_{cr} increases by increasing μ, i.e., increasing the positive dust concentration in the dusty plasma (also see Fig. 8, refer to the upper three curves therein, and Fig. 14), although this behavior becomes less dramatic and may even be reversed as ion temperature goes higher (see lower curve in Fig. 14).

VIII. CONCLUSIONS

We have undertaken an investigation of the envelope dynamics of nonlinearly modulated electrostatic (dust-acoustic) wavepackets in dusty plasmas characterized by the presence of a Maxwellian electron and a superthermal (kappa distributed) ion background. Both negative and positive dust charge cases were considered. A nonlinear Schrödinger equa-

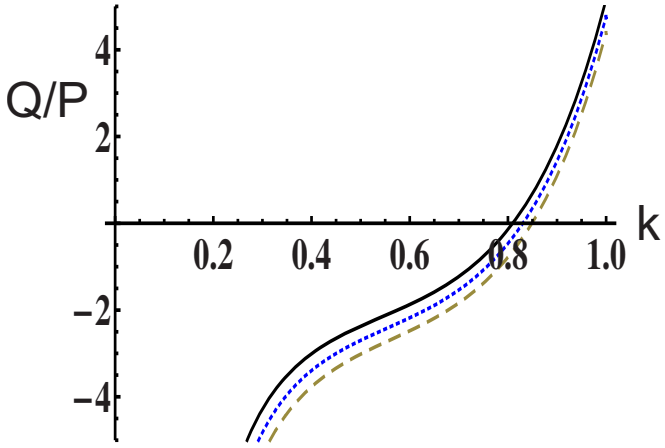

FIG. 13. (Color online) Variation of the ratio Q/P with the carrier wavenumber k for different values of μ and with $\kappa=2.5$, $\theta=0.1$, and $s=+1$ (positive dust). The solid curve corresponds to $\mu=1.25$, dotted curve to $\mu=1.5$, and dashed curve to $\mu=1.75$.

tion was derived for the wave amplitude, and exact expressions for the dispersion and (cubic) nonlinearity coefficients were obtained. These have allowed us to investigate the modulational (in)stability profile of dust-acoustic waves in various parameter regimes.

The influence of the relevant physical parameters (ion temperature, superthermality, dust concentration) on the dynamics has been traced by observing the effect of parameters θ, κ, μ (respectively) on

(a) the instability domain (i.e. the wavenumber threshold separating the stable and unstable carrier wavenumber regions),
(b) the envelope soliton characteristics (type, pulse width and height), and
(c) the growth rate of modulational instability.

The effect on the instability threshold is admittedly rather small for negative dust charge, but seems to be significant for positive dust. Superthermality leads to narrower (in spatial extension) bright or dark envelope solitons, although the effect on the bright case is less important.

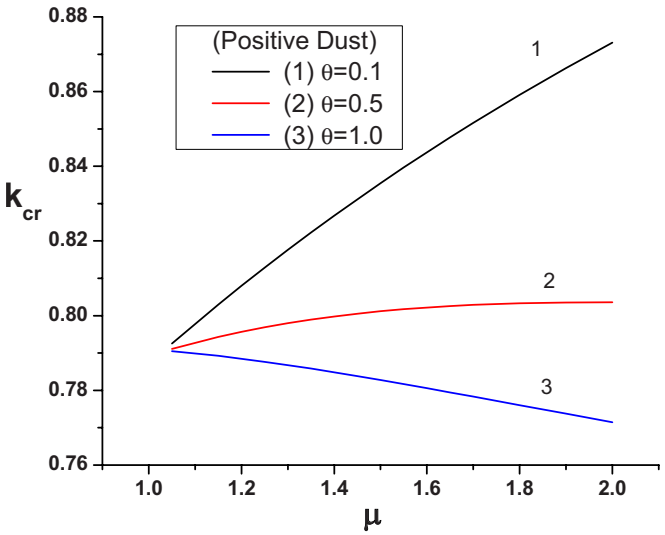

FIG. 14. (Color online) Variation of the instability (carrier wavenumber) threshold k_{cr} with the dust parameter μ (positive dust) for different values of θ and $\kappa=3$.

The growth rate of the modulational instability was also studied for different values of κ. The growth rate is significantly affected (and in fact reduced) by the superthermality and hence modulational instability can be controlled by the existence of a long tail in the plasma species distribution.

For large values of κ, say >6, the behavior of the wave-packet envelope amplitude seems to be almost as in Maxwellian plasmas, which corresponds to considering the expressions for c_1, c_2, and c_3 in the limit $\kappa\to\infty$. In this case, our results agree with earlier works for dust-acoustic waves against a thermal ions and electron background.

Our results may be relevant to existing and forthcoming experimental and space observations, where superthermal plasma distributions may be present.

ACKNOWLEDGMENTS

Professor Manfred Hellberg (University of KwaZulu-Natal, Durban, South Africa) is warmly acknowledged for a number of discussions on the kappa distribution. One of the authors (N.S.S.) thanks Guru Nanak Dev University, Amritsar, India for providing leave.

This work was supported by a UK EPSRC Science and Innovation award.

[1] C. K. Goertz, Rev. Geophys. **27**, 271, DOI: 10.1029/RG027i002p00271 (1989).
[2] D. A. Mendis and M. Rosenberg, Annu. Rev. Astron. Astrophys. **32**, 419 (1994).
[3] M. Horanyi, Astron. Astrophys. Rev. **34**, 383 (1996).
[4] F. Verheest, *Waves in Dusty Plasma* (Kluwer, Dordrecht, 2000).
[5] P. K. Shukla and A. A. Mamun, *Introduction to Dusty Plasma Physics* (Institute of Physics, Bristol, 2002).
[6] G. S. Selwyn, K. L. Haller, and E. F. Patterson, J. Vac. Sci. Technol. A **11**, 1132 (1993).
[7] H. Kersten, H. Deutsch, E. Stoffels, W. W. Stoffels, G. M. W. Kroesen, and R. Hippler, Contrib. Plasma Phys. **41**, 598 (2001).
[8] N. N. Rao, P. K. Shukla, and M. Y. Yu, Planet. Space Sci. **38**, 543 (1990).
[9] P. K. Shukla and V. P. Silin, Phys. Scr. **45**, 508 (1992).
[10] A. Barkan, R. L. Merlino, and N. D'Angelo, Phys. Plasmas **2**, 3563 (1995).
[11] E. Thomas, Jr., R. Fisher, and R. L. Merlino, Phys. Plasmas **14**, 123701 (2007).
[12] M. A. Hellberg, R. L. Mace, R. J. Armstrong, and G. Karlstad, J. Plasma Phys. **64**, 433 (2000).
[13] D. Summers and R. M. Thorne, Phys. Fluids B **3**, 1835 (1991).
[14] R. L. Mace and M. A. Hellberg, Phys. Plasmas **2**, 2098 (1995).
[15] R. L. Mace, M. A. Hellberg, and R. J. Treumann, J. Plasma Phys. **59**, 393 (1998).
[16] R. L. Mace, G. Amery, and M. A. Hellberg, Phys. Plasmas **6**, 44 (1999).
[17] M. A. Hellberg and R. L. Mace, Phys. Plasmas **9**, 1495 (2002).
[18] M. Hellberg, R. Mace, and T. Cattaert, Space Sci. Rev. **121**, 127 (2005).
[19] A. Hasegawa, K. Mima, and M. Duong-van, Phys. Rev. Lett. **54**, 2608 (1985).
[20] V. M. Vasyliunas, J. Geophys. Res. **73**, 2839, DOI: 10.1029/JA073i009p02839 (1968).
[21] P. Christon, D. G. Mitchell, D. J. Williams, L. A. Frank, C. Y. Huang, and T. E. Eastman, J. Geophys. Res. **93**, 2562, DOI: 10.1029/JA093iA04p02562 (1988).
[22] B. Abrahim-Shrauner and W. C. Feldman, J. Plasma Phys. **17**, 123 (1977).
[23] M. P. Leubner, J. Geophys. Res. **87**, 6335, DOI: 10.1029/JA087iA08p06335 (1982).
[24] T. P. Armstrong, M. T. Paonessa, E. V. Bell II, and S. M. Krimigis, J. Geophys. Res. **88**, 8893, DOI: 10.1029/JA088iA11p08893 (1983).
[25] M. P. Leubner, Phys. Plasmas **11**, 1308 (2004).

[26]A. Mushtaq and H. A. Shah, Phys. Plasmas **13**, 012303 (2006).
[27]N. Rubab and G. Murtaza, Phys. Scr. **73**, 178 (2006).
[28]H. Abbasi and H. H. Pajouh, Phys. Plasmas **14**, 012307 (2007).
[29]K. Aoutou, M. Tribeche, and T. H. Zerguini, Phys. Plasmas **15**, 013702 (2008).
[30]H. Abbasi and H. H. Pajouh, Phys. Plasmas **15**, 092902 (2008).
[31]H. Abbasi and H. H. Pajouh, Plasma Phys. Controlled Fusion **50**, 095007 (2008).
[32]L.-N. Hau and W.-Z. Fu, Phys. Plasmas **14**, 110702 (2007).
[33]R. A. Cairns, A. A. Mamun, R. Bingam, R. Bostrom, R. O. Dendy, C. M. C. Nairn, and P. K. Shukla, Geophys. Res. Lett. **22**, 2709, DOI: 10.1029/95GL02781 (1995).
[34]I. Kourakis and P. K. Shukla, J. Plasma Phys. **71**, 185 (2005).
[35]F. Verheest and R. S. Pillay, Phys. Plasmas **15**, 013703 (2008).
[36]J. Goree, Plasma Sources Sci. Technol. **3**, 400 (1994); C. Cui and J. Goree, IEEE Trans. Plasma Sci. **22**, 151 (1994).
[37]F. Melandso, Phys. Scr. **45**, 515 (1992).
[38]I. Kourakis and P. K. Shukla, Phys. Scr. **69**, 316 (2004).
[39]R. Tang and J. Xue, Phys. Plasmas **10**, 3800 (2003).
[40]I. Kourakis and P. K. Shukla, Nonlinear Processes Geophys. **12**, 407 (2005).
[41]T. Dauxois and M. Peyrard, *Physics of Solitons* (Cambridge University Press, Cambridge, 2005).
[42]R. Fedele and H. Schamel, Eur. Phys. J. B **27**, 313 (2002).
[43]R. Fedele, H. Schamel, and P. K. Shukla, Phys. Scr. **T98**, 18 (2002).
[44]O. Havnes, J. Trøim, T. Blix, W. Mortensen, L. I. Næsheim, E. Thrane, and T. Tønnesen, J. Geophys. Res. **101**, 10839, DOI: 10.1029/96JA00003 (1996).
[45]M. Horanyi, G. E. Morfill, and E. Grun, Nature (London) **363**, 144 (1993).
[46]A. H. Kim and R. L. Merlino, Phys. Plasmas **13**, 052118 (2006).
[47]A. A. Mamun and P. K. Shukla, Phys. Plasmas **10**, 1518 (2003).
[48]A. A. Mamun, and P. K. Shukla, Geophys. Res. Lett. **29**, 1870, DOI: 10.1029/2002GL015219 (2002).
[49]A. A. Mamun, Phys. Rev. E **77**, 026406 (2008).